Micro-cantilever testing on the short-term creep behaviour of cement paste at micro-scale

Yidong Gan, Matthieu Vandamme, Hongzhi Zhang, Yu Chen, Erik Schlangen, Klaas van Breugel, Branko Avija

Micro-cantilever testing on the short-term creep behaviour of cement paste at micro-scale

Yidong Gan [a], Matthieu Vandamme [b], Hongzhi Zhang [c,*] , Yu Chen [a], Erik Schlangen [a], Klaas van Breugel [a] and Branko Šavija [a].

[a] Microlab, Faculty of Civil Engineering and Geosciences, Delft University of Technology, Delft 2628, CN, The Netherlands

[b] Laboratoire Navier, UMR 8205, CNRS, École des Ponts ParisTech, IFSTTAR, Université Paris-Est, Champs-sur-Marne, France

[c] School of Qilu Transportation, Shandong University, 250002, Jinan, PR China

y.gan@tudelft.nl; matthieu.vandamme@enpc.fr; Y.Chen-6@tudelft.nl; Erik.Schlangen@tudelft.nl; K.vanBreugel@tudelft.nl; B.Savija@tudelft.nl;

* Corresponding author: hzzhang@mail.sdu.edu.cn

Abstract

This study proposes an experimental method for studying the short-term creep behaviour of cement paste at micro-scale. The micro-bending tests on miniaturized cantilever beams were used to characterize the viscoelastic properties of cement paste. The effects of w/b ratio, the type of binder and the stress level on the microscopic creep behaviour were investigated. It is found that the short-term creep of cement paste at microscale can be satisfactorily described by a power-law function. A linear viscoelastic behaviour has been observed in different cementitious systems at the microscale with the stress level up to 67.9%. When compared with the creep results in microindentation tests and conventional macroscopic tests, the obtained creep compliance function in this study is found to be both qualitatively and quantitatively representative of the macroscopic results. This experimental study underlines the importance of microstructural effect on the creep behaviours of cementitious materials at microscale.

Keywords: cement paste, creep, miniaturized cantilever beam, nanoindenter

1. Introduction

Ageing of infrastructure is considered to be a huge financial burden for modern industrialised societies [1]. One of the common ageing phenomena for concrete structures is creep [2]. Even though extensive research efforts has been devoted to it [3–7], this complicated phenomenon is still not fully understood. A comprehensive review of creep studies on cementitious materials indicates that despite the numerous influencing factors [8–13], the multiple time and length scales involved in the creep process further exacerbate the complexity [14–16].

In view of the duration of creep test, there are usually short-term creep tests ranging from several minutes to months [17–20] and long-term creep tests lasting from several months to years

[5,8,16]. In these tests, at least two distinct creep kinetics have been identified, i.e. the power-law creep and the logarithmic creep [5,14,20–23]. It is often argued that the short-term and long-term creep may be governed by different mechanisms [3,16,24]. For the short-term creep, the creep behaviour is thought to be associated with the water movement and redistribution [24], whilst for the long-term creep, the underlying creep mechanism is debatable and various theories have been proposed [2,3,7,12,13,24,25]. Nevertheless, many researchers believe that the rearrangement of calcium–silicate–hydrate (C-S-H), e.g. sliding and compaction, plays a dominant role in the long-term creep [2,3,12,26]. Note that none of these theories alone can explain all the experimental observations and it appears that several of the proposed physical processes could occur simultaneously [3,24,27]. Admittedly, both short-term and long-term creep tests are essential to the integrated understanding and prediction of creep behaviour [14].

Concrete is a multiscale heterogeneous composite and the creep phenomenon can be observed at different length scales, i.e. from the hydrate to concrete [2,14,20]. In the context of multiscale modelling [19,28], the experimental techniques intended to characterize the viscoelastic properties of elemental constituents at every scale should be well developed. While most studies focus on the macroscopic creep tests of cement paste and concrete [6,8,29–32], there are some studies conducted on the characterization of the viscoelastic properties at nano and micro-scale using the indentation technique [14,20,33–35]. Vandamme and Ulm [2,20] performed nanoindentation creep tests directly on the C-S-H structures, which is usually recognized as the main creeping phase in cementitious materials [12,26], and they suggested a qualitative analogy with the creep of soils. Wei et al [21] also investigated the creep behaviour of cement paste across the nanometre to micrometre scale by using the indentation technique. These minutes-long indentation creep tests enable a rapid quantitative assessment of the long-term creep properties of cementitious materials [14,20]. However, a major limitation of this technique is that such indentation tests do not provide the access to characterize the short-term creep behaviour [14,17,22]. Vandamme [27] suggested that this is because of the high magnitude of stresses below the indenter tip. Therefore, in order to gain a complete description of creep behaviour at small scale, the complementary test methods capable of evaluating the microscopic short-term creep behaviour are needed. This can be achieved by small-scale testing of miniature specimens, which has already been used in the determination of mechanical properties [36–43]. In literature, there are mainly two techniques for generating small-scale samples, i.e. the Focused Ion Beam

technology (FIB) and the micro dicing method. Note that the investigated length scale is different for these two methods. For the FIB technique, the length of the generated micro-beam is around 20 μm. Consequently, each micro-beam comprises a single component of cement paste, namely the inner and outer hydration products and portlandite (CH) [41]. However, for the micro dicing method adopted in this study, the fabricated beams are relatively larger with the size of 300 μm × 300 μm × 1650 μm. The fabricated beam is thus composed of clinker (ranging from 0 μm to 150 μm), hydration products (mainly consisting of CH and inner and outer products with size roughly smaller than 100 μm) and pores of various sizes. The prepared miniaturized specimens are then loaded using the nanoindenter to investigate their mechanical response. By applying constant loading on these small-scale specimens, it is also possible to assess their creep properties.

The main objective of this work is to explore the short-term viscoelastic properties of cement paste at micro-scale by means of micro-bending tests on miniaturized cantilever beams. The proposed test method was first validated using glass beams, which are expected to be made of a homogenous and isotropic material. Then the results in creep tests were carefully interpreted considering the possible additional deformation mechanisms existing in current test method. Several parameters, such as the w/c ratio, stress level and the addition of ground granulated blast furnace slag (GGBFS) were examined in this study. Finally, the obtained results in this study were compared with the results of indentation tests and macroscopic creep tests.

2. Materials and methods

2.1. Materials and experimental procedure

2.1.1 Materials

In this study, the materials used were standard grade CEM I 42.5 N Portland cement, GGBFS and deionized water. Two series of paste specimens were prepared. The first one is the pure OPC paste with water/cement ratios of 0.3, 0.4, and 0.5. For the second series, the cement paste was blended with GGBFS with the replacement level of 70% by mass. In the blended cement paste w/b ratios of 0.3 and 0.4 were used. The fresh paste was first cast in plastic cylindrical moulds with 24 mm diameter and 39 mm height. Afterwards, the paste was rotated at a speed of 2.5 rpm at room temperature (26 °C) for 24 h to mitigate the influence of bleeding. All specimens were cured in sealed conditions at room temperature for 28 days. At the end of the curing period, the hardened cement paste was demoulded and then cut into slices with a thickness of 3 mm. Before

further grinding, the samples were kept in isopropanol to stop the hydration process. For the detailed description of arresting hydration using the solvent exchange method, the reader is referred to [36].

2.1.2 Preparation of micro-cantilever beams

Micro-cantilever beams (MCB) were prepared using a precision micro-dicing machine (MicroAce Series 3 Dicing Saw), which is generally applied to cut semiconductor wafers. Prior to the preparation of cantilever beams, the slices of cement paste were first ground to obtain two smooth and parallel surfaces. In the grinding process, two grinding discs of 135 μm and 35 μm were used in sequence. After reaching the designed thickness of 2.15 mm, the micro-dicing machine was used to apply two perpendicular cutting directions and the same cutting space on the samples. In this way, multiple rows of cantilever beams, including at least 30 beams, with a square cross section of 300 μm × 300 μm were generated. The cutting depth, i.e. the cantilevered length, was approximately 1.65 mm ± 0.01 mm. The cutting process is schematically shown in Figure 1. Some of the prepared beams were then examined by using an environmental scanning electron microscope (ESEM). An overall accuracy for the cross-sectional dimensions of ±2 μm can be reached with the fabrication process (Figure 2). Precautions were also taken to minimize carbonation of the samples before testing by storing the beams in an isopropanol solution. As the drying histories of beams may significantly affect their creep behaviour [6], all samples were prepared according to the same procedure and exposed to the same relative humidity (RH) during the tests. The porosity of miniaturized sample made of OPC has been examined using the X-ray computed tomography (XCT) in the author's previous work [44]. The porosity for OPC with different w/c ratios (0.3, 0.4 and 0.5) was found to be 8.44%, 11.84% and 17.5%, respectively. For blended cement paste with slag, similar specimens using CEM III/B were also examined by XCT [45]. The porosity for different w/b ratios (0.3, 0.4 and 0.5) was found to be 5.73%, 7.89% and 9.79%, respectively. However, it should be noted that due to the limitation of image resolution in XCT (2 μm/voxel in this case), pores smaller than 2 μm cannot be detected and are mixed within the segmented solid phases. Therefore, the porosity measured by XCT is much lower compared to porosity measured by the mercury intrusion porosimetry (MIP) [46], For instance, the MIP results of OPC with the w/c ratios of 0.3, 0.4 and 0.5 are 17%, 23% and 31%, respectively.

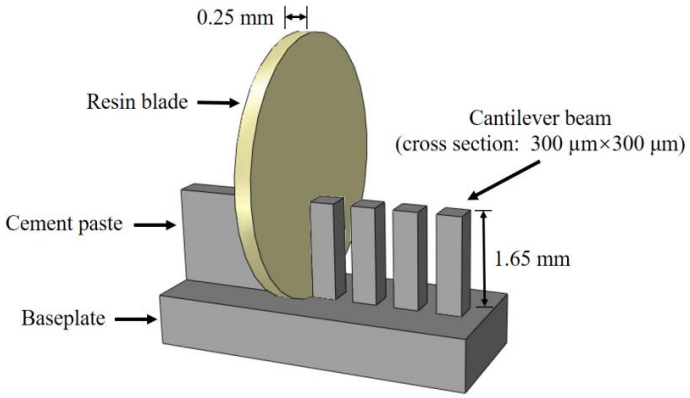

Figure 1: Schematic diagram of sample preparation.

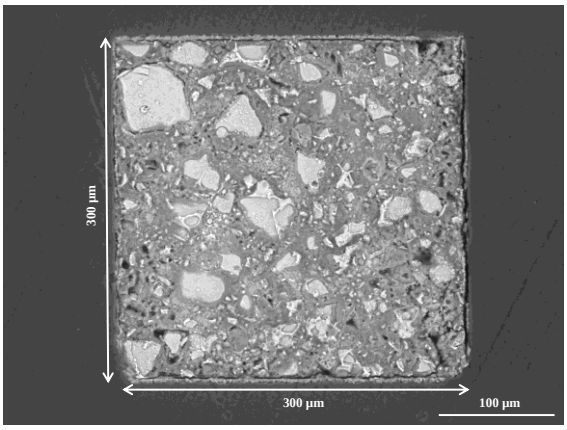

Figure 2: ESEM image of the cross-sections of cantilever beam.

2.2 Micro-cantilever bending test

2.2.1 Mechanical properties

A KLA Nano indenter G200 was used to conduct bending tests on the MCBs. The baseplate of beams was first attached on a flat metal surface using cyanoacrylate adhesive. A cylindrical wedge indenter tip (Figure 3) with a length of 200 μm was used to apply vertical line loads at the free end of the beams. Before testing, the angle and center of the tip are always calibrated by probing into the aluminium. Afterwards, the angle of MCB is carefully adjusted under the in-situ microscope in the nanoindenter to ensure that the line load is applied perpendicularly to the length direction of beam. The loading procedure for characterization of the mechanical properties is displacement controlled and the loading rate is 50 nm/s. All tests were conducted in a well-insulated chamber preventing any significant change of temperature and RH during the test. The average measured temperature and RH during the tests were 27.2 ± 0.7 °C and 31.0% ± 1.3%, respectively. The experimental set-up is schematically shown in Figure 4. For each

material composition, 30 cantilever beams were monotonically loaded to failure. The load-displacement curves were recorded and used to determine the elastic modulus and flexural strength. A typical load-displacement curve for the static test is shown in Figure 5. It can be seen that the displacement of the beams linearly increases with the load till failure occurs. The maximum load was used to calculate the flexural strength according to Equation (1).

$$f_{\mathrm{t}} = \frac{F_{\max} dh}{2I} \tag{1}$$

where d is the measured distance between the load point and the fracture point, h is the side length of the square cross-section, and $I=h^4/12$ is the moment of inertia. The linear portion of the load-displacement curve was used to determine the elastic modulus according to Equation (2):

$$E = \frac{kL^3}{3I} \tag{2}$$

where L is the length of the cantilever beam, which equals the distance between the load point and the fixed end; k is the slope measured from the linear region of the load-displacement curve.

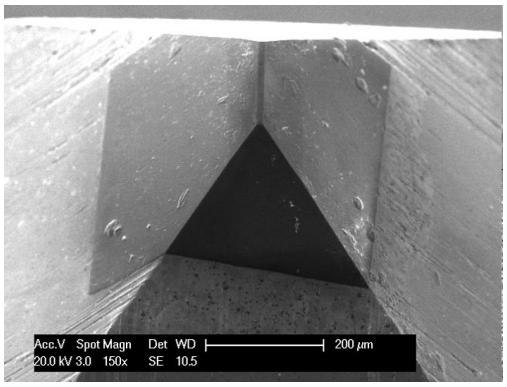

Figure 3: ESEM micrograph of the diamond cylindrical wedge tip.

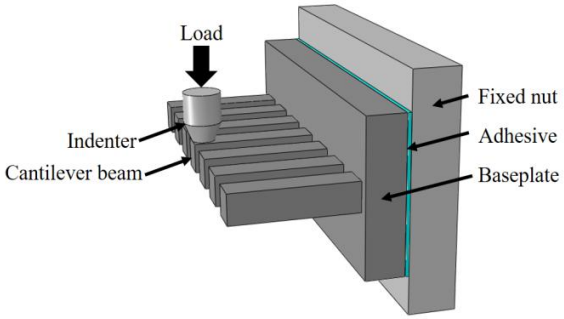

Figure 4: Schematic diagram of test set-up.

Since the nanoindenter recodes the displacement of the tip head instead of directly measuring the beam deflection, the measured total displacement may also contain the additional deformation

during the loading stage, such as the penetration depth of the indenter tip and the deformation of the baseplate and the adhesive layer. Therefore, the measured displacement should be calibrated considering the additional deformation, otherwise the calculated elastic modulus will be underestimated [47]. By using the finite element modelling method, the effects of the baseplate and the adhesive layer on the total deformation can be quantified [39]. The simulation results indicate that 14% and 0.5% of the measured displacement is caused by the deformation of the baseplate and the adhesive layer, respectively. These additional displacements will be excluded in the determination of the elastic modulus. Moreover, as pointed out by many researchers [17,31], the actual elastic modulus will always be underestimated as the displacements measured in the loading phase are not only elastic but also include some viscoelastic deformation. Nevertheless, as long as the loading rate is fast enough, the creep deformation during the loading stage can be neglected with respect to the considerably larger elastic deformation [17]. For the sake of simplicity, the plastic deformation during the loading stage, e.g. the indentation depth, is also not considered in the determination of elastic modulus.

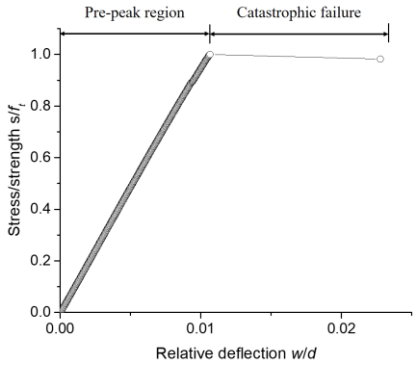

Figure 5: Typical load-displacement curves of static tests

2.2.2 Short-term creep behaviour

In creep tests, a loading protocol consisting of three stages was used to acquire sufficient information for the analysis of creep phenomenon. Firstly, the MCBs were loaded in a fully elastic regime, i.e. 30% of the strength, to determine the apparent elastic modulus using the Equation (2). Afterwards, the beams were subjected to a constant load to assess the viscoelastic responses of MCBs. Before the creep test, the samples were kept in the chamber for temperature equalization until the thermal drift rate is below 0.05nm/s. The load was then increased to the predefined value at a constant rate of 2 mN/s and held for 800 seconds, see Figure 6. Note that the thermal drift after the creep test was also measured but not considered in this study, as the

measured drift may be affected by the creep recovery [48]. In addition, tests with three different stress levels (from 12.5% to 67.9%) were also performed to check whether the cementitious material at this scale behaves in a linear viscoelastic manner. An example of a displacement-time curve is shown in Figure 7. After the constant loading tests, the tested beams were statically loaded to failure in order to assess the residual flexural strength. At least 15 samples were tested for each material composition and test series. All the creep tests were performed in the well-insulated chamber with continuously recorded RH and temperature at 30 s intervals.

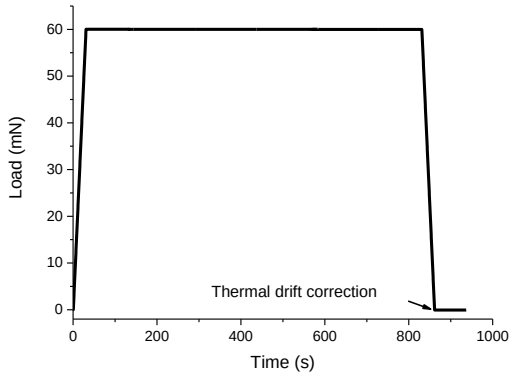

Figure 6: Loading history of creep tests for w/c 0.3 OPC under the load level of 60mN.

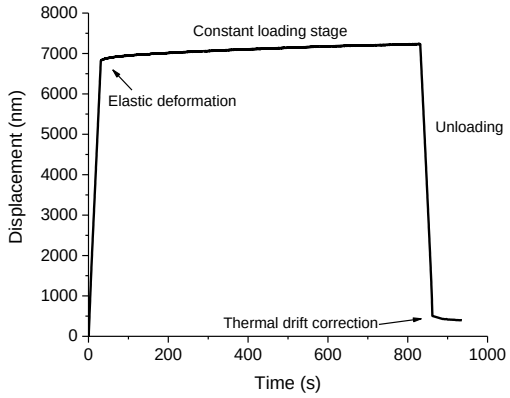

Figure 7: Typical displacement-time curve for creep test

Since the deformation mechanisms of cementitious material under constant loading are very complex, the experimental data should be carefully interpreted. In particular, it is known that moisture exchange occurs between the concrete and the environment under drying condition, leading to drying shrinkage and drying creep [11]. Therefore, special precaution of the hydraulic equilibrium was taken in this study by continuously monitoring the weight loss of the companion sample during the creep tests. It is found that due to the extremely thin cross-section with the

volume to surface ratio of only 0.07 mm, the MCBs quickly equilibrated to the ambient RH prior to the tests. It is well known that the size of specimen indicated by the volume to surface ratio considerably affects the drying process [49]. Moreover, based on the weight measurements of the companion MCBs, it is found that there is almost no weight loss during the short-term creep tests. As a negligible change of temperature and relative humidity is also expected, the thermal strain, drying shrinkage and drying creep during the creep tests can be ignored [11,19,50]. Moreover, in consideration of the test duration and age of samples (28 days) used in this study, the autogenous shrinkage caused by hydration can also be neglected [29]. Therefore, the basic creep compliance $J(t,t_0)$ can be written as:

$$J(t,t_0) = \frac{\varepsilon_{\mathrm{el}} + \varepsilon_{\mathrm{bc}}(t,t_0)}{\sigma} \tag{3}$$

where $\varepsilon_{\mathrm{el}}$ is the instantaneous strain at the end of loading phase, which is assumed to be identical with the elastic strain in this study; $\varepsilon_{\mathrm{bc}}(t,t_0)$ is the specific basic creep strain at time t, t_0 is the time at the beginning of constant loading; σ is the maximum stress at the fixed end of the beam. For the flexural creep tests, it is assumed that cross-sections of beams remain plane under the applied stress levels. This is based on the observations of previous static tests, where the deflection of beams linearly increases with the load up to failure, see Figure 5. Therefore, the compressive and tensile creep strains are assumed to develop equally with a linear distribution along the height of beams. This has also been experimentally identified in macroscopic flexural creep tests on concrete beams loaded at 50% of the strength [32]. According to the classical beam theory and Hooke's law, the elastic strain at the top or bottom surface of a beam can be calculated as:

$$\varepsilon_{el} = \frac{3\delta_{el}h}{2L^2} \tag{4}$$

where δ_{el} is the measured displacement at the end of loading phase. By defining the creep coefficient $\varphi(t,t_0)$ as the ratio of basic creep strain to the initial elastic strain, its value can be determined by the measured deflection $\delta(t)$ as follows [29,51]:

$$\varphi(t,t_0) = \frac{\varepsilon_{bc}(t,t_0)}{\varepsilon_{el}} = \frac{\delta(t) - \delta_{el}}{\delta_{el}} \tag{5}$$

Afterwards, the specific basic creep compliance $C(t,t_0)$ can be calculated as:

$$C(t,t_0) = \frac{\varphi(t,t_0)\varepsilon_{\mathrm{el}}}{\sigma} \tag{6}$$

Generally, the effect of self-weight of cement paste should be considered when calculating the

creep compliance [29,51]. However, in our study the self-weight of MCB only accounts for 0.002% of the load-induced moment at the fixed end of beam, thus the stress generated by self-weight of the beam is not considered in this study. In addition, it is assumed that the measured time-dependent deflection is affected by the baseplate in a similar way as the elastic deformation, i.e. 14% of total deformation (see Section 2.2.1). This is also taken into consideration in the calculation of creep strain.

2.3 Validation of test method

In order to examine the validity of the proposed test method to characterize the creep behaviour of cement paste, a comparative study was conducted, in which the MCBs made of commercial objective glass with identical geometrical size (1650 μm × 300 μm × 300 μm) were fabricated using the same preparation procedure described in section 2.1.2. Generally, the glass is expected to exhibit no creep at room temperature [52]. Hence, any measured time-dependent deformation for glass tests should be attributed to the inherent drift of the equipment or test set-up. The typical curves of change in displacement with respect to the holding time for both the cement paste and glass beams are compared in Figure 8. It is shown that the measured time-dependent deformation for glass beams is very small compared to that of the cement paste beams. Also, MCBs with higher w/c ratio exhibit higher creep displacement. This certifies that the test method is able to evaluate the viscoelastic behaviour of materials. To quantify the intrinsic drift, five glass beams were used as references and tested under the same constant load for each test series. For instance, the average intrinsic drift rate of the glass beams, which includes any drift of the apparatus and creep of the adhesive layer in particular, under the highest load (60 mN) was 0.0789 nm/s ± 0.0066 nm/s with a CoV of 8.4%. The total drift over an 800 s period was 63.12 nm ± 5.28 nm, which is around 6% - 13% of the deflection of cement paste beams. Hereby, for all the creep tests on cement paste, the measured creep displacements were adjusted to account for the intrinsic drift rate according to the following equation:

$$\delta_{\mathrm{c}}(t) = \gamma[\delta_{\mathrm{m}}(t) - \delta_{\mathrm{d}}(t)] \tag{7}$$

where $\delta_{\mathrm{c}}(\mathrm{t})$, $\delta_{\mathrm{m}}(t)$ and $\delta_{\mathrm{d}}(t)$ are the corrected creep displacement, measured creep displacement and drift displacement, respectively; γ is the coefficient accounting for the effects of the baseplate, which is 0.86 in this study.

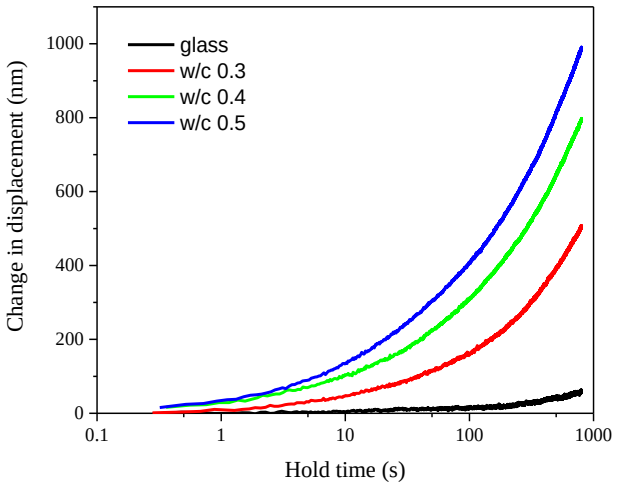

Figure 8: Comparison of the change in displacement for glass and cement paste beams

In addition, the possible time dependent penetration depth of the indenter during the constant loading was also investigated. However, it seems difficult to distinguish the penetration depth from the total displacement due to the heterogeneity of indented material and the specific boundary conditions used in this study. Here, we performed a series of tests to indirectly examine the development of indentation depth under the constant load. The analysis rests on the hypothesis that the indentation depth, if it is at the same order of magnitude with beam deflection, should randomly vary with the loading locations because of the different local microstructures. Therefore, for each MCB, 10 parallel positions with an identical space (i.e. 30 μm) near the free end of beam were selected as the loading points. To minimize the effect of shear deformation, longer beams, i.e. 1800 μm, were used. A trapezoidal load history with a maximum load of 20 mN and a holding period of 20 s were applied on each loading point. The applied stress level was around 20% of strength to ensure the individual tests staying within the elastic limit. In this way, the change of displacements during the constant loading were obtained for each loading point. Afterwards, the changes of displacements with respect to the loading distance were fitted by a power law function passing through the origin, see Figure 9. It is found that for each MCB the fitted line for measured changes of displacements at different loading points has a determination coefficient of 0.92. This small variation implies that the indentation creep displacement does exist but is insignificant compared to the total creep displacement. It proves that the obtained creep deformation mainly originates from the beam deflection and the penetration depth is, therefore, neglected in this study.

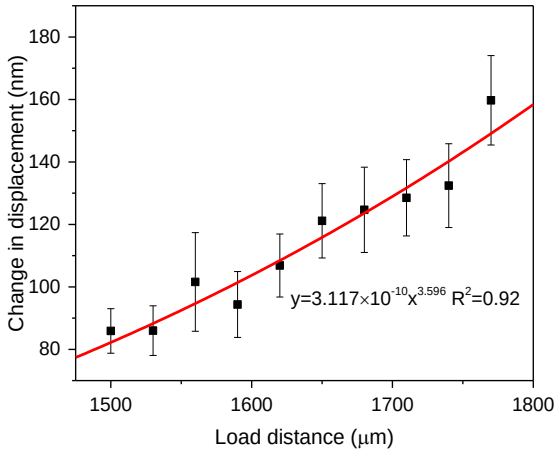

Figure 9: The variation of change in displacement with different loading distance

3. Results

3.1 Mechanical properties

For the monotonic loading tests, the flexural strength and static elastic modulus were obtained and shown in Table 1. The presented results are the average of 30 duplicate samples. The obtained mechanical properties are in good agreement with the results presented in literature [36,39]. For different w/b ratios, samples with higher w/b ratio exhibit lower strength and elastic modulus. The scatter of results, indicated by the coefficient of variation (CoV), increases with the w/b ratio. For the same w/b ratio, the mechanical properties of samples blended with GGBFS were slightly lower than the OPC samples at 28 days. Since the rate of hydration of blast-furnace slag mixed with water is initially lower than that of Portland cement, the blended cement paste containing blast-furnace slag shows lower strength at early age but similar or greater strength at later ages [53,54].

Table 1: The mechanical properties measured from the static tests

Material	w/b ratio	Static elastic modulus (GPa)	Flexural strength (MPa)
100% OPC	0.3	19.54 ± 1.49 (7.6%)	28.03 ± 2.67 (9.5%)
	0.4	16.19 ± 1.93 (11.9%)	23.32 ± 2.76 (11.8%)
	0.5	10.82 ± 2.51 (23.1%)	16.94 ± 3.73 (22.1%)
30% OPC + 70% GGBFS	0.3	17.01 ± 1.14 (6.7%)	25.43 ± 1.81 (7.1%)
	0.4	14.14 ± 1.57 (11.1%)	21.76 ± 3.01 (13.8%)
	0.5	8.99 ± 1.42 (15.8%)	14.25 ± 3.14 (22.1%)

3.2 Specific basic creep compliance

The specific basic creep compliance at 800 s for different w/b ratios and type of binders are shown in Figure 10. It can be seen that samples with higher w/b ratio exhibit larger basic creep compliance. The dependence of the creep behaviour on the w/c ratio is well known. Either the water content or the porosity of samples is believed to be the main reason for this [37,55–57]. For a given w/b ratio, the basic creep compliance of samples blended with 70% slag is higher than the pure cement paste in this study. This is mostly related to the development of microstructure as also reflected by the mechanical properties. However, it should be noted that in the long-term, the addition of GGBFS may lead to similar or less basic creep due to the ongoing hydration [54].

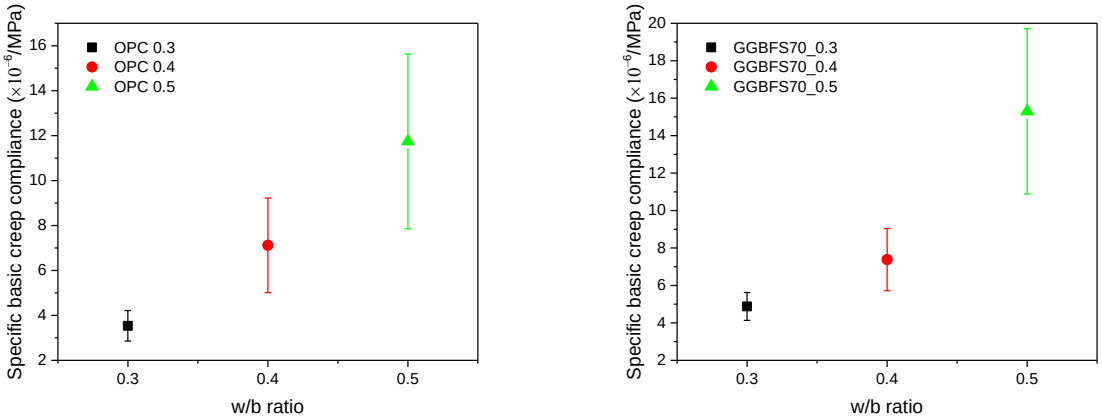

Figure 10: The specific basic creep compliance measured at 800 s.

Figure 11 shows the evolution of specific creep compliance with respect to time for OPC beams with three w/c ratios. Note that the hold time in the plots refers to the time elapsed under the constant loading. When plotted in log-log scale, the curves of specific creep compliance are almost linear in spite of the small fluctuation in the first few seconds. This representation of the results indicates that the development of creep compliance during the time period tested (800s) can be fitted by a power-law creep function [6,17,19]:

$$C(t,t_0) = \alpha\left(\frac{t-t_0}{t_1}\right)^{\beta} \quad (8)$$

where t_0 is the age of the sample when the load reached the constant value; $t-t_0$ is the time elapsed under constant loading; t_1 is the time unit, i.e. 1 s. The α and β are fitting parameters, where α corresponds to the specific basic creep compliance at 1 second. For each case, the power function parameters were determined with a correlation coefficient greater than 0.99. Note that

the creep deformation during the loading stage is not considered in the creep function. The calculated apparent elastic modulus and two fitting parameters α and β for all test series are summarized in Table 2. It can be seen that the calculated apparent elastic modulus based on the loading slope of curves were almost identical with the static elastic modulus, as the two similar loading rates were used. The variability of apparent elastic modulus, in terms of CoV, are also consistent with the static elastic modulus for different w/b ratios and compositions. In addition, the parameter α as well as its standard deviation were found to increase with increasing w/b ratio. On the contrary, the exponent β varies a little and appears to be independent of w/b ratios and type of binder. This has also been reported in macroscopic tests [6,17,19] on cement paste. Moreover, when compared with the apparent elastic modulus for the same material composition, the variabilities of creep tests are larger.

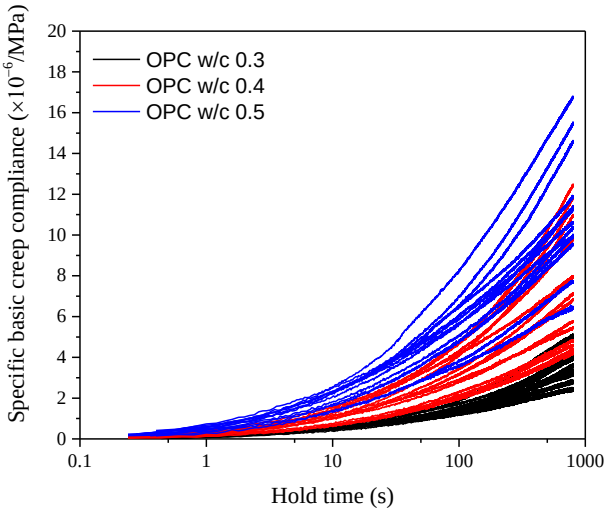

Figure 11: The specific basic creep compliance with respect to the logarithmic time

Table 2: Apparent elastic modulus and fitting parameters α and β in Eq.(8)

Material	w/b	$E_{apparent}$ (GPa)	α	β	Average R^2
100% OPC	0.3	19.64 ± 1.20 (6.1%)	0.23 ± 0.03 (13.6%)	0.39 ± 0.04 (10.7%)	0.9970
	0.4	15.49 ± 1.49 (9.6%)	0.51 ± 0.07 (15.0%)	0.39 ± 0.04 (10.8%)	0.9971
	0.5	10.20 ± 2.51 (21.4%)	1.19 ± 0.29 (24.6%)	0.36 ± 0.02 (5.2%)	0.9935
30% OPC + 70% GGBFS	0.3	18.75 ± 1.66 (8.8%)	0.31 ± 0.04 (13.2%)	0.39 ± 0.02 (5.4%)	0.9987
	0.4	15.03 ± 1.67 (11.2%)	0.55 ± 0.08 (15.4%)	0.38 ± 0.03 (7.8%)	0.9964
	0.5	9.22 ± 1.50 (16.2%)	1.24 ± 0.23 (18.5%)	0.39 ± 0.05 (14.4%)	0.9987

The rate of specific basic creep compliance with respect to time is shown in Figure 12. The decreasing trend with a slope around 0.61-0.64 is found in all creep tests. Zhang et al. [14]

compared the rate of creep compliance between the macroscopic compressive tests and the microindentation tests on cement paste at the early stage of creep tests. It has been reported [5,14] that for 0.38 w/c cement paste the slopes of creep compliance rate curves in macroscopic tests and microindentation tests were 0.51 and 0.99, respectively. It seems that the obtained creep compliance rate in this study is closer to the results of macroscopic tests.

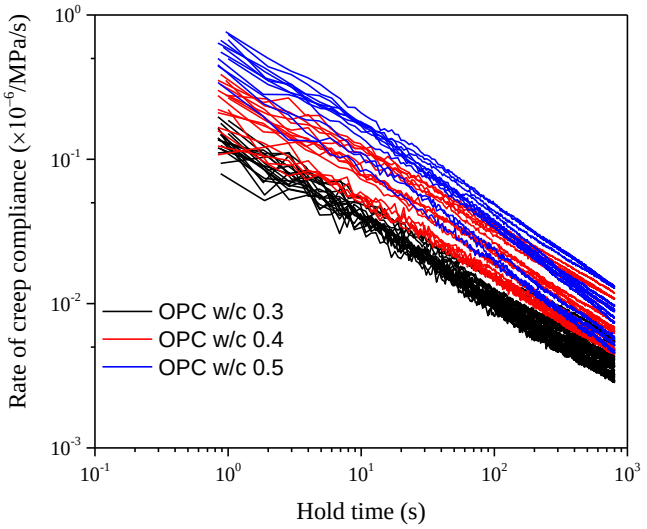

Figure 12: The creep rate of cement pastes with different w/c ratios

Figure 13 illustrates the effect of stress level on the measured ultimate creep strain at 800s for w/b 0.4 OPC and blended paste. A linear relationship was found between the ultimate creep strain and the stress level (from 12.5% to 67.9%). This indicates a linear viscoelastic characteristic of cement paste at this length scale, which further proves that the developments of microcracking and indentation depth during the constant loading are insignificant in current tests. To the best knowledge of the authors, the linear viscoelasticity of cement paste has never been examined microscopically. This examination cannot be accomplished by indentation tests because the magnitude of the stresses below the indenter is independent of the applied maximal load due to the self-similarity of the indenter [20]. For flexural creep tests at larger scale, several studies [29,30,32,58] have confirmed that concrete beams with w/c from 0.3 to 0.5 exhibit linear creep under the stress level below 40% - 50% of strength.

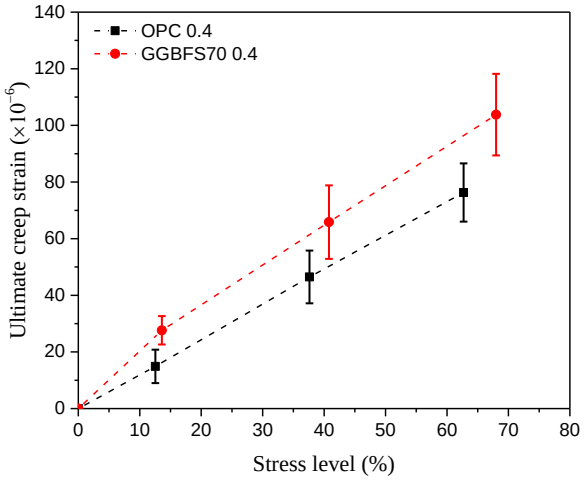

Figure 13: The effect of stress level on ultimate creep strain at 800 s for two paste series with w/b of 0.4.

4. Discussion

4.1 On the variability of test results.

At the micro-scale, multiple solid phases and varying amounts of gel pores (<0.01 μm), capillary pores (0.01 μm-10 μm) and air voids (>10 μm) are recognised in the hardened cement paste. Hence, the variability in the measured data essentially arises from the selected small sampling volumes of this highly heterogeneous material. Nevertheless, it is still necessary to analyse the additional sources of variability of results, which also helps to gain a better understanding of the material behaviour at this scale. It is not surprising to see that the mechanical properties decrease with the increase of w/c ratio mainly because of the increasing capillary porosity [37,55–57]. However, it is also found that the variation of both elastic modulus and flexural strength, in terms of CoV, increases with the w/c ratio. Similar observations have also been reported in other types of small-scale tests [36,39,42]. This is probably attributed to the pore size distributions for different w/c ratios. It should be noted that due to the small sampling volume (300 μm × 300 μm × 1650 μm) used in this study, the effect of capillary pores (0.1 μm-10 μm) on the mechanical properties of MCBs becomes more evident. According to the MIP test results from [46,57,59], the mean pore radius increases with the w/c ratio. It means that the largest size of the capillary pores would be larger for higher w/c ratio, whereas the smallest gel pores remain almost the same. Consequently, the dispersion range of the pore size for higher w/c ratio would be wider. Therefore, the higher w/c ratio may result in a wider range of capillary porosity and hence a

larger variability of mechanical properties. This explanation also holds for the blended cement paste with GGBFS at the age of 28 days [60].

For the same material composition, the mean value and CoV of the apparent elastic modulus measured prior to the creep tests are almost consistent with that of static elastic modulus. However, there is a larger variation found in the results of creep tests, e.g. the ultimate creep compliance at 800 s (Figure 10) and the fitting parameter α (Table 2). This seems reasonable as there are different mechanisms involved in the elastic deformation and creep deformation of cement paste. It is well known that the elastic modulus mainly depends on the porosity of material [61], while the creep mechanism of cement paste is much more complicated and depends on many factors. For the short term creep mechanism, several researchers [9,62] suggested that the creep deformation may be due to a stress-induced redistribution of capillary water within the pore structure of cement paste. However, it should be noted that the state of water in cement paste considerably depends on the relative humidity [63,64]. In consideration of the RH (31%) used in this study, the pore walls of the pore system, i.e. the surfaces of the colloidal hydration products, are covered with one single mono-molecular layer of water [63]. Thus, the gel water instead of capillary water should play a dominant role in the creep process. According to several proposed creep mechanisms in literature [12,13,25], the creep of cement paste is largely affected by the movement and distribution of the gel water. In this context, it seems plausible that factors affecting the distribution and transport of moisture, such as the connectivity of pore structure, may lead to a larger variation of creep results.

4.2 The power law function of creep

The fact that the evolution of creep compliance can be expressed by a power function, at least for the short term creep tests, has been observed in numerous macroscopic experiments for both cement paste [6,17–19] and concrete [8,31,65]. A common finding of these short-term tests is that the power-law exponent β is less sensitive to the compositions compared to the fitting parameter α. For the cement paste, the range of variation for the exponent β reported in the literature is very small, with most values falling between 0.20 and 0.40, which is very close to the results in the current study, i.e. 0.36-0.39. More interestingly, a range of values between 0.30 and 0.45 has also been observed in concrete samples [31,65]. Moreover, Königsberger [28] demonstrated, by using the downscaling homogenization method, that the hydrates at smaller

scale also exhibit a single power-law function with a creep exponent being surprisingly close to the results tested in different cement pastes.

On the contrary, the parameter α, which corresponds to the creep compliance at unit time, is found to be largely affected by the compositions of cement paste, degree of hydration and moisture content [6,17–19]. It is also demonstrated by the multiscale studies of cementitious materials that the constituents and microstructures significantly influence the macroscopic viscoelastic behaviour [3,28,31,66,67]. At nanometre scale, Vandamme [2,20] stated that the creep behaviour of the hydrated phases is largely determined by the packing density of C-S-H particles. At the micro-scale, the cement paste is composed of the intrinsically viscoelastic C-S-H gel particles, porosity and non-creeping inclusions, such as other hydration products and unhydrated clinker. The macroscopic creep behaviour of cement paste is, therefore, determined by the interactions among all these constituents. In particular, the porosity and non-creeping inclusions influence the creep mainly by altering the internal stress field and moisture distribution [19,28,67]. From this point of view, the apparent elastic modulus and residual strength, which also depend on the porosity and volume fractions of inclusions, may be helpful to interpret the creep results. Therefore, the relationships between the mechanical properties and the inverse of parameter α in this study are plotted in Figure 14 (a) and (b). The inverse of α also refers to the so-called creep modulus [17,20]. It can be seen that the inverse of α increases with the increasing mechanical properties following a power-law function. Moreover, the scaling relations are found to be independent of the w/c ratio and the addition of slag. These observations are similar to the results in nanoindentation tests [2,20], in which the scaling relations between the creep modulus and indentation properties are found to be independent of the w/c, the heat treatment, or the addition of silica fumes or filler. Moreover, the calculated contact creep modulus of C-S-H in nanoindentation tests is a power function of the indentation modulus and linearly related to the indentation hardness [20]. These unique relationships imply that there seems a common contributor that controls the overall elastic, plastic and viscoelastic deformation at the investigated length scale, such as the gel or capillary porosity [2,20]. The underlying microstructural effect on the creep behaviour could be properly demonstrated using numerical approaches at different scales [15,19,67].

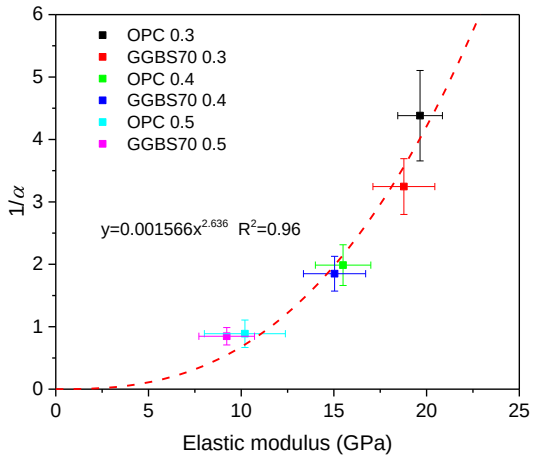

(a)

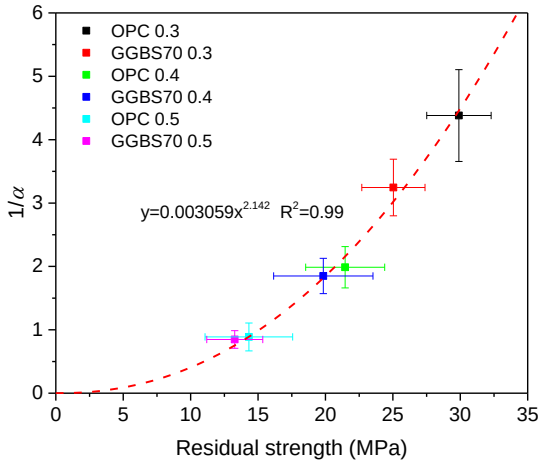

(b)

Figure 14: The relationship between the inverse of α and (a) the elastic modulus, and (b) the residual flexural strength

4.3 The comparisons with microindentation and macroscopic tests

In several experimental studies [29,30,32,51,58], it has been found that for the short-term creep, the specific basic creep compliance measured in flexural creep tests could be compared directly with the results in compressive creep tests, as they have similar order of magnitude during the first few days. Here, the creep functions obtained in MCB bending tests, microindentation tests [14,22] and macroscopic compressive tests [5,6,19] with similar material compositions and loading age are directly compared and plotted in Figure 15. Even though the probed area in microindentation tests [14,22] is almost at the same length scale with MCBs, a large quantitative discrepancy is found in the measured specific basic creep compliance, see Figure 15(a). For

instance, the specific creep compliance of microindentation tests at 1000 s are almost two orders of magnitude higher than the results in MCB bending tests. Moreover, there is also a significant qualitative difference between these two tests. In microindentation tests, the obtained creep functions follow a short initial transition phase and a subsequent logarithmic creep. However, in this study, the power-law creep instead of logarithmic creep was observed.

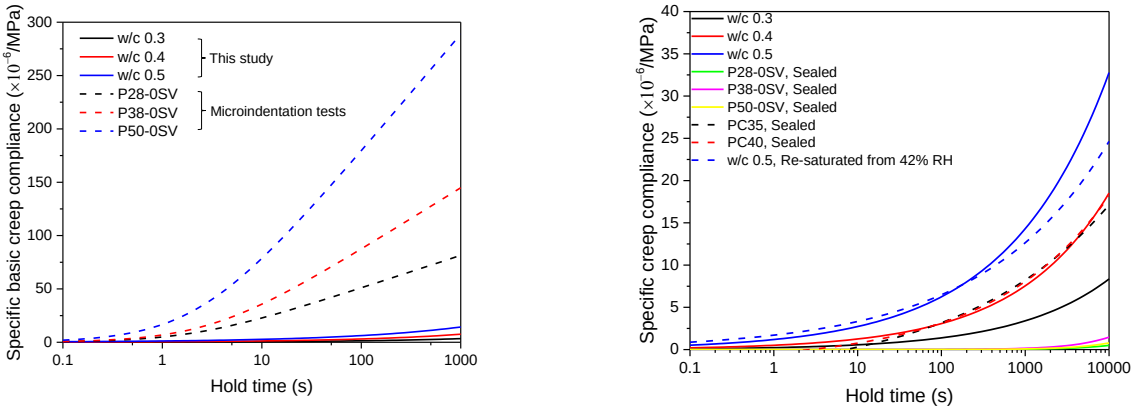

(a) (b)

Figure 15: The comparison with (a) microindentation tests [14] and (b) macroscopic tests [6,14,19]. The numbers after the 'P' or 'PC' represent the w/c ratio.

This phenomenological feature of creep, i.e. the logarithmically evolved creep function, is believed to be associated with the long-term creep mechanism [9,20,68]. It can be captured in indentation test after only several seconds [14,20,35], while it costs days or even months for macroscopic cement paste [14] or concrete samples [23,68] to reach the logarithmic creep. Vandamme [20,69] suggests that the fact that the logarithmic creep can be captured in such a short time is probably because of the high magnitude of applied stresses in indentation tests, where the stress below the indenter is on the order of a few hundred MPa to around 1GPa [69]. This is much higher than the generally applied stress in macroscopic tests and is assumed to significantly decrease the activation energies of the local microscopic relaxation sites, thus decreasing the characteristic time for long-term creep [69]. In this context, the creep function measured in this study should be more comparable with the macroscopic tests due to the equivalent applied stresses, i.e. 10 -30 MPa. As can be seen in Figure 15(b), the creep functions obtained in this study are very close to the most macroscopic results in literature despite the results in [14]. Note that a logarithmic function was used in [14], which appears to poorly fit the very initial part of specific basic creep compliance [17]. Therefore, the experimental data in

terms of specific basic creep compliance at 0.1 day (i.e. 8640 s) were directly compared and displayed in Figure 16. The observed consistency of the results confirms that the measured creep compliance in MCB bending tests are more representative for macroscopic tests regardless of the length scale. This is promising, as the creep behaviour of cementitious materials can be readily characterized by using the small-scale tests. Moreover, as suggested by [14,17], since the complete creep function is composed of initial short-term creep, described by a power-law function, and subsequent long-term creep, described by a logarithmic creep function, it might be possible to perform the small scale tests proposed in this study together with the indentation tests in [14,20] to fully characterize the creep function of cement paste at microscale.

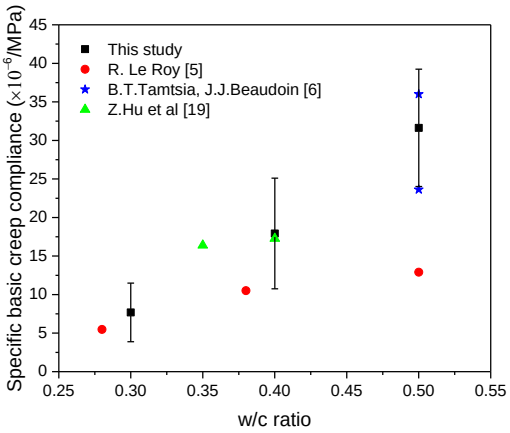

Figure 16: The comparison with the specific basic creep compliance in macroscopic tests at 0.1 day.

4.4 Limitations and perspectives

Some limitations of the current method should be pointed out. Since the miniaturized samples are inevitably exposed to the ambient conditions during the tests, carbonation must have occurred at the surface layer of beams [70]. This is considered extremely important, especially with regard to the thin cross-sections adopted in this study, as substantial carbonation can significantly affect the deformations and microstructures of cement paste [71]. Note that the effect of carbonation may be more apparent in blended cement paste [71]. It is also expected that the short test duration and low RH used in this study may limit the effect of carbonation in the creep process, but the role of carbonation probably becomes more significant in the long-term creep tests. Another concern of the presented test method is that damage induced by shrinkage has been introduced in the samples before the tests, which may further increase uncertainties of the tests results [6]. The samples with different w/b ratios even exposed to the same RH may

accumulate different levels of damage during the drying process. Therefore, more efforts are needed to quantify the effects of both carbonation and initial damage on the creep behaviour. With regard to the sources of uncertainty, some of them may also originate from the imperfect contact between the indenter tip and sample. In addition, it should be mentioned that, for the short-term creep tests in this study, the effect of thermal drift is reduced to some extent by performing a stabilization period prior to the creep test. However, for the long-term tests, the effect of thermal drift may largely affect the results and there is no guarantee that the thermal drift will remain constant during the long-term test. Therefore, the application of indentation instruments may be limited for performing long-term measurements owing to the thermal drift. Nevertheless, the current test method offers distinct advantages for characterizing the short-term creep at microscale and provides experimental data for validation and calibration of multiscale modelling approaches [28,36,72]. It is recommended, therefore, that future work should focus on the combination of numerical and experimental investigations of the creep behaviour of cementitious materials at different scales.

Conclusions

In this paper, minutes long micro-bending tests on miniaturized cantilever beams were used to characterize the short-term creep behaviour of cement paste with different w/c ratios and types of binder. The following conclusions can be drawn from the presented experimental studies:

- The proposed test method fills the experimental gap in characterizing the microscopic short-term creep properties and also provides valuable insight into the creep behaviour of cementitious materials at microscale.
- Even though it is well known that the creep intrinsically originates from the C-S-H nanostructure, the good correlation between the mechanical properties and creep compliance rate found in this study suggests that microstructural features may largely impact the creep behaviour of cement paste at micro-scale.
- By comparing with the microindentation tests and conventional macroscopic compressive creep tests on cement paste, it is shown that the micro-scale bending tests are both qualitatively and quantitatively representative of macroscopic tests. The differences of obtained creep between indentation tests and the current tests are assumed to be related to the different applied stress levels, but further supporting evidence is still needed.

- The evolution of short-term specific basic creep compliance of cement paste with different compositions can be captured appropriately by a power-law function with a constant exponent. This is in line with findings in macroscopic tests. It is suggested that by combining the short-term creep function obtained in this study with the long-term creep function captured in microindentation tests, a complete non-ageing creep function at microscale can be obtained.

Acknowledgements

Yidong Gan, Hongzhi Zhang and Yu Chen would like to acknowledge the funding supported by China Scholarship Council under grant number 201706130140, 201506120067 and 201807720005, respectively. Mr. Arjan Thijssen is also gratefully acknowledged for his help with the ESEM experiments.

Reference

[1] K. van Breugel, D. Koleva, T. van Beek, The ageing of materials and structures: Towards scientific solutions for the ageing of our assets, 2017. doi:10.1007/978-3-319-70194-3.

[2] M. Vandamme, F.J. Ulm, Nanogranular origin of concrete creep, Proc. Natl. Acad. Sci. U. S. A. 106 (2009) 10552–10557. doi:10.1073/pnas.0901033106.

[3] H. Ye, Creep Mechanisms of Calcium–Silicate–Hydrate: An Overview of Recent Advances and Challenges, Int. J. Concr. Struct. Mater. 9 (2015) 453–462. doi:10.1007/s40069-015-0114-7.

[4] Z.R. Bažant, G.H. Li, Comprehensive database on concrete creep and shrinkage, ACI Mater. J. 105 (2008) 635–637.

[5] R. Le Roy, Déformations instantanées et différées des bétons à hautes performances, (PhD Thesis) Ec. Natl. Des Ponts Chaussées. (1996).

[6] B.T. Tamtsia, J.J. Beaudoin, Basic creep of hardened cement paste. A re-examination of the role of water, Cem. Concr. Res. 30 (2000) 1465–1475. doi:10.1016/S0008-8846(00)00279-9.

[7] P. Klug, F. Wittmann, Activation energy of creep of hardened cement paste, Matériaux Constr. 2 (1969) 11–16. doi:10.1007/BF02473650.

[8] P. Rossi, J.L. Tailhan, F. Le Maou, Creep strain versus residual strain of a concrete loaded under various levels of compressive stress, Cem. Concr. Res. 51 (2013) 32–37. doi:10.1016/j.cemconres.2013.04.005.

[9] F.H. Wittmann, Shrinkage and Creep of Concrete: Mechanisms as Described on Different Structural Levels, Syst. Concr. Sci. Technol. through Multi-Scale Model. (2015).

[10] Z.P. Bazant, M.H. Hubler, Theory of cyclic creep of concrete based on Paris law for fatigue growth of subcritical microcracks, J. Mech. Phys. Solids. 63 (2014) 187–200. doi:10.1016/j.jmps.2013.09.010.

[11] G. Pickett, The Effect of Chang in Moisture-Content on the Creep of Concrete Under a Sustained Load, ACI J. Proc. 38 (1942) 333–357. doi:10.14359/8607.

[12] Z.P. Bažant, A.B. Hauggaard, S. Baweja, F.J. Ulm, Microprestress-solidification theory for concrete creep. I: Aging and drying effects, J. Eng. Mech. 123 (1997) 1188–1194. doi:10.1061/(ASCE)0733-9399(1997)123:11(1188).

[13] T.C. Powers, The thermodynamics of volume change and creep, Matériaux Constr. 1 (1968) 487–507. doi:10.1007/BF02473638.

[14] Q. Zhang, R. Le Roy, M. Vandamme, B. Zuber, Long-term creep properties of cementitious materials: Comparing microindentation testing with macroscopic uniaxial compressive testing, Cem. Concr. Res. 58 (2014) 89–98. doi:10.1016/j.cemconres.2014.01.004.

[15] Q.H. Do, S. Bishnoi, K.L. Scrivener, Microstructural Modeling of Early-Age Creep in Hydrating Cement Paste, (2016). doi:10.1061/(ASCE)EM.1943-7889.0001144.

[16] O. Bernard, F.J. Ulm, J.T. Germaine, Volume and deviator creep of calcium-leached cement-based materials, Cem. Concr. Res. 33 (2003) 1127–1136. doi:10.1016/S0008-8846(03)00021-8.

[17] M. Irfan-Ul-Hassan, B. Pichler, R. Reihsner, C. Hellmich, Elastic and creep properties of young cement paste, as determined from hourly repeated minute-long quasi-static tests, Cem. Concr. Res. 82 (2016) 36–49. doi:10.1016/j.cemconres.2015.11.007.
[18] B.T. Tamtsia, J.J. Beaudoin, J. Marchand, The early age short-term creep of hardening cement paste : load-induced hydration effects, 26 (2004) 481–489. doi:10.1016/S0958-9465(03)00079-9.
[19] Z. Hu, A. Hilaire, J. Ston, M. Wyrzykowski, P. Lura, K. Scrivener, Intrinsic viscoelasticity of C-S-H assessed from basic creep of cement pastes, Cem. Concr. Res. 121 (2019) 11–20. doi:10.1016/j.cemconres.2019.04.003.
[20] M. Vandamme, F.J. Ulm, Nanoindentation investigation of creep properties of calcium silicate hydrates, Cem. Concr. Res. 52 (2013) 38–52. doi:10.1016/j.cemconres.2013.05.006.
[21] Y. Wei, S. Liang, X. Gao, Indentation creep of cementitious materials: Experimental investigation from nano to micro length scales, Constr. Build. Mater. 143 (2017) 222–233. doi:10.1016/j.conbuildmat.2017.03.126.
[22] Q. ZHANG, Creep properties of cementitious materials: effect of water and microstructure. An approach by microindentation, (2014).
[23] Z.P. Bažant, M.H. Hubler, Q. Yu, Pervasiveness of excessive segmental bridge deflections: Wake-up call for creep, ACI Struct. J. 108 (2011) 766–774.
[24] F.H. Wittmann, Creep and shrinkage mechanisms, Creep Shrinkage Concr. Struct. (1982) 129–161.
[25] W. Ruetz, A hypothesis for the creep of hardened cement paste and the influence of simultaneous shrinkage, Proc. Struct. Concr. Its Behav. under Load. (1968) 365–387.
[26] H.M. Jennings, Colloid model of C-S-H and implications to the problem of creep and shrinkage, Mater. Struct. Constr. 37 (2004) 59–70.
[27] M. Vandamme, M. Vandamme, Two models based on local microscopic relaxations to explain long-term basic creep of concrete Subject Areas : Author for correspondence :, (2018).
[28] M. Königsberger, M. Irfan-ul-Hassan, B. Pichler, C. Hellmich, Downscaling based identification of nonaging power-law creep of cement hydrates, J. Eng. Mech. 142 (2016) 1–11. doi:10.1061/(ASCE)EM.1943-7889.0001169.
[29] Y. Wei, D. Ph, M. Asce, Z. Wu, J. Huang, S. Liang, Comparison of Compressive , Tensile , and Flexural Creep of Early-Age Concretes under Sealed and Drying Conditions, 30 (2018) 1–13. doi:10.1061/(ASCE)MT.1943-5533.0002495.
[30] S. Liang, Y. Wei, Methodology of obtaining intrinsic creep property of concrete by flexural deflection test, Cem. Concr. Compos. 97 (2019) 288–299. doi:10.1016/j.cemconcomp.2019.01.003.
[31] L. Su, Y. feng Wang, S. qi Mei, P. fei Li, Experimental investigation on the fundamental behavior of concrete creep, Constr. Build. Mater. 152 (2017) 250–258. doi:10.1016/j.conbuildmat.2017.06.162.
[32] N. Ranaivomanana, S. Multon, A. Turatsinze, Basic creep of concrete under compression , tension and bending, Constr. Build. Mater. 38 (2013) 173–180. doi:10.1016/j.conbuildmat.2012.08.024.
[33] C. Pichler, R. Lackner, Identification of Logarithmic-Type Creep of Calcium-Silicate-Hydrates by Means of Nanoindentation, (2009) 17–25.
[34] J. Němeček, Creep effects in nanoindentation of hydrated phases of cement pastes, Mater. Charact. 60 (2009) 1028–1034. doi:10.1016/j.matchar.2009.04.008.
[35] C.A. Jones, Z.C. Grasley, Short-term creep of cement paste during nanoindentation, Cem. Concr. Compos. 33 (2011) 12–18. doi:10.1016/j.cemconcomp.2010.09.016.
[36] H. Zhang, B. Šavija, S.C. Figueiredo, E. Schlangen, Experimentally validated multi-scale modelling scheme of deformation and fracture of cement paste, Cem. Concr. Res. 102 (2017) 175–186. doi:10.1016/j.cemconres.2017.09.011.
[37] H. Zhang, B. Šavija, E. Schlangen, Combined experimental and numerical study on micro-cube indentation splitting test of cement paste, Eng. Fract. Mech. 199 (2018) 773–786. doi:10.1016/j.engfracmech.2018.04.018.
[38] H. Zhang, Y. Gan, Y. Xu, S. Zhang, E. Schlangen, B. Šavija, Experimentally informed fracture modelling of interfacial transition zone at micro-scale, Cem. Concr. Compos. 104 (2019) 103383. doi:10.1016/j.cemconcomp.2019.103383.
[39] Y. Gan, H. Zhang, B. Šavija, E. Schlangen, K. van Breugel, Static and Fatigue Tests on Cementitious Cantilever Beams Using Nanoindenter, Micromachines . 9 (2018). doi:10.3390/mi9120630.
[40] H. Zhang, B. Šavija, Y. Xu, E. Schlangen, Size effect on splitting strength of hardened cement paste: Experimental and numerical study, Cem. Concr. Compos. 94 (2018) 264–276. doi:10.1016/j.cemconcomp.2018.09.018.

[41] J. Němeček, V. Králík, V. Šmilauer, L. Polívka, A. Jäger, Tensile strength of hydrated cement paste phases assessed by micro-bending tests and nanoindentation, Cem. Concr. Compos. 73 (2016) 164–173. doi:10.1016/j.cemconcomp.2016.07.010.
[42] H. Zhang, B. Šavija, S.C. Figueiredo, M. Lukovic, E. Schlangen, Microscale testing and modelling of cement paste as basis for multi-scale modelling, Materials (Basel). 9 (2016). doi:10.3390/ma9110907.
[43] H. Zhang, Y. Xu, Y. Gan, Z. Chang, E. Schlangen, B. Šavija, Combined experimental and numerical study of uniaxial compression failure of hardened cement paste at micrometre length scale, Cem. Concr. Res. 126 (2019). doi:10.1016/j.cemconres.2019.105925.
[44] H. Zhang, B. Šavija, E. Schlangen, Towards understanding stochastic fracture performance of cement paste at micro length scale based on numerical simulation, Constr. Build. Mater. 183 (2018) 189–201. doi:10.1016/j.conbuildmat.2018.06.167.
[45] B. Šavija, H. Zhang, E. Schlangen, Micromechanical testing and modelling of blast furnace slag cement pastes, Constr. Build. Mater. 239 (2020). doi:10.1016/j.conbuildmat.2019.117841.
[46] R.A. Cook, K.C. Hover, Mercury porosimetry of hardened cement pastes, 29 (1999) 933–943.
[47] L.S. Stephens, K.W. Kelly, S. Simhadri, A.B. McCandless, E.I. Meletis, Mechanical property evaluation and failure analysis of cantilevered LIGA nickel microposts, J. Microelectromechanical Syst. 10 (2001) 347–359. doi:10.1109/84.946780.
[48] M. Gan, V. Tomar, Role of length scale and temperature in indentation induced creep behavior of polymer derived Si-C-O ceramics, Mater. Sci. Eng. A. 527 (2010) 7615–7623. doi:10.1016/j.msea.2010.08.016.
[49] J.A. Almudaiheem, W. Hansen, Effect of Specimen Size and Shape on Drying Shrinkage of Concrete., ACI Mater. J. 84 (1987) 130–135.
[50] W. HANSEN, Drying Shrinkage Mechanisms in Portland Cement Paste, J. Am. Ceram. Soc. 70 (1987) 323–328. doi:10.1111/j.1151-2916.1987.tb05002.x.
[51] C.H. Un, J.G. Sanjayan, R.S. Nicolas, J.S.J. Van Deventer, Mini-Beam Test for Assessing the Creep Trend of Paste, Mortar, and Concrete, CONCREEP 2015 Mech. Phys. Creep, Shrinkage, Durab. Concr. Concr. Struct. - Proc. 10th Int. Conf. Mech. Phys. Creep, Shrinkage, Durab. Concr. Concr. Struct. (2015) 1350–1359. doi:10.1061/9780784479346.160.
[52] W. Cooke, P. Howell, Viscoelastic behaviour of glass and "fictive temperature," Math. Ind. 372 (1998) 22. http://www.maths-in-industry.org/miis/372/.
[53] G. Men, V. Bonavetti, E.F. Irassar, Strength development of ternary blended cement with limestone filler and blast-furnace slag, 25 (2003) 61–67.
[54] E. Özbay, M. Erdemir, H.I. Durmuş, Utilization and efficiency of ground granulated blast furnace slag on concrete properties - A review, Constr. Build. Mater. 105 (2016) 423–434. doi:10.1016/j.conbuildmat.2015.12.153.
[55] R. Kumar, B. Bhattacharjee, Porosity, pore size distribution and in situ strength of concrete, Cem. Concr. Res. 33 (2003) 155–164. doi:10.1016/S0008-8846(02)00942-0.
[56] I. Odler, M. Rößler, Investigations on the relationship between porosity, structure and strength of hydrated Portland cement pastes. II. Effect of pore structure and of degree of hydration, Cem. Concr. Res. 15 (1985) 401–410. doi:10.1016/0008-8846(85)90113-9.
[57] G. Ye, Experimental study and numerical simulation of the development of the microstructure and permeability of cementitious materials, 2003.
[58] N. Ranaivomanana, S. Multon, A. Turatsinze, Tensile, compressive and flexural basic creep of concrete at different stress levels, Cem. Concr. Res. 52 (2013) 1–10. doi:10.1016/j.cemconres.2013.05.001.
[59] B. Kondraivendhan, B. Bhattacharjee, Effect of Age and Water-Cement Ratio on Size and Dispersion of Pores in Ordinary Portland Cement Paste, (2011).
[60] N. De Belie, J. Kratky, S. Van Vlierberghe, Influence of pozzolans and slag on the microstructure of partially carbonated cement paste by means of water vapour and nitrogen sorption experiments and BET calculations, Cem. Concr. Res. 40 (2010) 1723–1733. doi:10.1016/j.cemconres.2010.08.014.
[61] D.P.H. HASSELMAN, Relation Between Effects of Porosity on Strength and on Young's Modulus of Elasticity of Polycrystalline Materials, J. Am. Ceram. Soc. 46 (1963) 564–565. doi:10.1111/j.1151-2916.1963.tb14615.x.
[62] E.J. SELLEVOLD, C.W. RICHARDS, Short-Time Creep Transition for Hardened Cement Paste, J. Am. Ceram. Soc. 55 (1972) 284–289. doi:10.1111/j.1151-2916.1972.tb11285.x.
[63] K. Van Breugel, Simulation of hydration and formation of structure in hardening cement-based materials., (1993).
[64] J.J. Thomas, S.A. FitzGerald, D.A. Neumann, R.A. Livingston, State of Water in Hydrating Tricalcium

Silicate and Portland Cement Pastes as Measured by Quasi-Elastic Neutron Scattering, J. Am. Ceram. Soc. 84 (2004) 1811–1816. doi:10.1111/j.1151-2916.2001.tb00919.x.
[65] F.H. Wittmann, J. Lukas, The Application of Rate Theory to Time-Dependent Deformation of Concrete, Mag. Concr. Res. 26 (1974) 191–197. doi:10.1680/macr.1974.26.89.191.
[66] M. Irfan-ul-hassan, M. Königsberger, R. Reihsner, C. Hellmich, M. Asce, B. Pichler, A.M. Asce, How Water-Aggregate Interactions Affect Concrete Creep : Multiscale Analysis, 7 (2017) 1–16. doi:10.1061/(ASCE)NM.2153-5477.0000135.
[67] A.B. Giorla, C.F. Dunant, Microstructural effects in the simulation of creep of concrete, Cem. Concr. Res. 105 (2018) 44–53. doi:10.1016/j.cemconres.2017.12.001.
[68] J.M. Torrenti, R. Le Roy, Analysis of some basic creep tests on concrete and their implications for modeling, Struct. Concr. 19 (2018) 483–488. doi:10.1002/suco.201600197.
[69] M. Vandamme, Two models based on local microscopic relaxations to explain long-term basic creep of concrete Subject Areas : Author for correspondence :, (2018).
[70] V. Rostami, Y. Shao, A.J. Boyd, Z. He, Microstructure of cement paste subject to early carbonation curing, Cem. Concr. Res. 42 (2012) 186–193. doi:10.1016/j.cemconres.2011.09.010.
[71] B. Šavija, M. Luković, Carbonation of cement paste: Understanding, challenges, and opportunities, Constr. Build. Mater. 117 (2016) 285–301. doi:10.1016/j.conbuildmat.2016.04.138.
[72] S. Scheiner, C. Hellmich, A.M. Asce, Continuum Microviscoelasticity Model for Aging Basic Creep of Early-Age Concrete, 135 (2009).